Journal of Structural Biology 191 (2015) 365–375

Contents lists available at ScienceDirect

Journal of Structural Biology

journal homepage: www.elsevier.com/locate/yjsbi

High resolution structures of *Plasmodium falciparum* GST complexes provide novel insights into the dimer–tetramer transition and a novel ligand-binding site

Markus Perbandt [a,c,e,*,1], Raphael Eberle [a,1], Lena Fischer-Riepe [b], Huaixing Cang [d], Eva Liebau [b], Christian Betzel [a,e]

[a] Institute of Biochemistry and Molecular Biology, University of Hamburg, Laboratory of Structural Biology of Infection and Inflammation, c/o DESY, Notkestr. 85, Build. 22a, D-22603 Hamburg, Germany
[b] Department of Molecular Physiology, University of Münster, Schlossplatz 8, D-48143 Münster, Germany
[c] Institute of Medical Microbiology, Virology and Hygiene, University Medical Center Hamburg-Eppendorf (UKE), D-20246 Hamburg, Germany
[d] Institute of Biophysics, Chinese Academy of Sciences, Beijing, China
[e] The Hamburg Centre for Ultrafast Imaging, Luruper Chaussee 149, D-22761 Hamburg, Germany

ARTICLE INFO

Article history:
Received 4 March 2015
Received in revised form 8 June 2015
Accepted 9 June 2015
Available online 10 June 2015

Keywords:
Malaria
Glutathione S-transferase
GST
Tetramerization
Ligandin
Non-substrate binding site

ABSTRACT

Protection from oxidative stress and efficient redox regulation are essential for malarial parasites which have to grow and multiply rapidly in pro-oxidant rich environments. Therefore, redox active proteins currently belong to the most attractive antimalarial drug targets. The glutathione S-transferase from *Plasmodium falciparum* (*Pf*GST) is a redox active protein displaying a peculiar dimer–tetramer transition that causes full enzyme-inactivation. This distinct structural feature is absent in mammalian GST isoenzyme counterparts. A flexible loop between residues 113–119 has been reported to be necessary for this tetramerization process. However, here we present structural data of a modified *Pf*GST lacking loop 113–119 at 1.9 Å resolution. Our results clearly show that this loop is not essential for the formation of stable tetramers. Moreover we present for the first time the structures of both, the inactive and tetrameric state at 1.7 Å and the active dimeric state in complex with reduced glutathione at 2.4 Å resolution. Surprisingly, the structure of the inactive tetrameric state reveals a novel non-substrate binding-site occupied by a 2-(N-morpholino) ethane sulfonic acid (MES) molecule in each monomer. Although it is known that the *Pf*GST has the ability to bind lipophilic anionic ligands, the location of the *Pf*GST ligand-binding site remained unclear up to now.

1. Introduction

Malaria is among the most prevalent infectious diseases in the developing world, imposing a vast burden of mortality and perpetuating cycles of poverty (WHO, 2010). The control of malaria is challenged by drug resistance and new antimalarial drugs are urgently needed (Perez et al., 2012). The parasite *Plasmodium falciparum* causes malaria tropica, the most prevailing parasitic disease worldwide. The emergence of strains resistant to drugs used for prophylaxis and treatment and no vaccine available makes the characterization of alternative drug targets an urgent requirement (Greenwood and Mutabingwa, 2002; Olliaro, 2001).

Sophisticated defense strategies have evolved in parasitic organisms that enable them to deal with a broad range of foreign and endogenously toxic compounds. *P. falciparum* parasites utilize host proteins as food source during their erythrocytic stage and large quantities of hemoglobin are digested, confronting the parasite with high amounts of toxic hemin. Thus, the discovery of compounds selectively inhibiting the detoxification of hemin is of high importance for the development of novel antimalarial drugs.

Glutathione S-transferases (GSTs) [EC 2.5.1.18] play a key role in detoxification processes. On the basis of amino acid sequence homology, immunological cross reactivity, substrate specificity and variation of active site residues, GSTs can be grouped into

Abbreviations: *Pf*GST, *Plasmodium falciparum* glutathione S-transferase; GSH, glutathione; G-site, glutathione-binding site; H-site, xenobiotic substrate-binding site; L-site, ligand-binding site; MES, 2-(N-morpholino) ethanesulfonic acid.

* Corresponding author at: Institute of Biochemistry and Molecular Biology, University of Hamburg, Laboratory of Structural Biology of Infection and Inflammation, c/o DESY, Notkestr. 85, Build. 22a, D-22603 Hamburg, Germany.
E-mail address: markus.perbandt@uni-hamburg.de (M. Perbandt).

[1] Both authors contributed equally to the work.

http://dx.doi.org/10.1016/j.jsb.2015.06.008
1047-8477/

different classes (Frova, 2006). They catalyze the nucleophilic addition of the tripeptide glutathione (GSH) to a large variety of nonpolar or toxic compounds and thereby enhance the solubility and excretion of the resulting products. GSTs are functional and stable dimers and the active site is composed of two neighboring substrate-binding sites. The so called G-site binds reduced glutathione and the hydrophobic H-site can accommodate a variety of electrophilic co-substrates (Hayes et al., 2005; Mannervik and Danielson, 1988). Several crystal structures of the wild-type GST from *P. falciparum* (*Pf*GST) are already known (Fritz-Wolf et al., 2003; Hiller et al., 2006; Perbandt et al., 2004; Tripathi et al., 2007). Although the overall three-dimensional structure is homologue to other known GST isoforms, the *Pf*GST could not be clearly assigned to any of the specified GST classes.

Previous studies revealed that the *Pf*GST is an important intracellular ligandin and is able to efficiently bind large lipophilic molecules like bilirubin, hemin and certain drugs (Axarli et al., 2004; Deponte and Becker, 2005; Harwaldt et al., 2002). Distinct ligand-binding sites have been described for GSTs from different organisms (Ji et al., 1996; McTigue et al., 1995; Oakley et al., 1999; Prade et al., 1997; Reinemer et al., 1996). While the localization of the *Pf*GST ligand-binding site (L-site) has not been structurally described so far, it was proposed to be part of the H-site or the inter-subunit cleft (Liebau et al., 2002., 2005).

Two properties of the *Pf*GST never observed in other members of the GST superfamily are of particular interest and underline the outstanding significance of this enzyme. Firstly, the enzyme shows a strong positive homotropic behavior that modulates the hemin affinity of the two subunits (Liebau et al., 2005). Secondly, in the absence of GSH the *Pf*GST gets inactivated in a relative short period of time and loses its ability to bind hemin (Liebau et al., 2005).

This inactivation process is known to be related to a dimer–tetramer transition of the protein (Fritz-Wolf et al., 2003; Hiller et al., 2006; Tripathi et al., 2007). The dimer–tetramer transition has not been observed for any other GST (Liebau et al., 2009). In the absence of reduced GSH or other ligands, two active dimers form a tetramer. The homodimers are interlocked with each other by loop 113–119 which occupy the H-site of the other monomer and vice versa. Loop 113–119 connects two conserved α-helices and bears the TNLFKQN sequence. The PfGST is the only enzyme of the GST superfamily, which is present as a tetramer rather than a dimer. It was already reported that truncation, increased rigidity or even a simple point mutation of this loop causes a dramatic decrease in the tetramerization kinetics (Liebau et al., 2009). It was also proposed that an interaction between Asn112 and Lys117 plays a key role in keeping the tetramer structure stable (Quesada-Soriano et al., 2014).

Here we report for the first time the high resolution structure of *Pf*GST in the active dimeric state in complex with GSH. Furthermore, based on the structural analysis of three different crystal structures of *Pf*GST in both, the active and inactive state, our obtained results extend the knowledge concerning the requirements for the dimer–tetramer-transition and provide novel insights with respect to the ability of the enzyme to bind lipophilic and toxic substances, thereby securing the inactivation and immobilization of these compounds.

2. Material and methods

2.1. Recombinant expression and purification of the PfGST

*Pf*GST was cloned, expressed and purified as reported previously (Burmeister et al., 2003; Liebau et al., 2002; Perbandt et al., 2004). After 4 h growth at 37 °C, bacterial cells were harvested by centrifugation; the cell pellet was dissolved in 100 mM Tris/HCl buffer pH 8.5 and sonicated. The cell lysate was centrifuged at 16.000×*g* and 4 °C for 1 h. The supernatant was mixed with Superglu glutathione superflow resin (Generon, Berkshire, UK) and incubated for 1 h at 4 °C. Unspecific bound proteins were removed by washing the matrix with 10× bed volumes of 100 mM Tris/HCl buffer, pH 8.5 and the recombinant protein was eluted with reduced GSH. Cloning, recombinant expression and purification of the mutant *Pf*GST$^{\Delta 114–118}$ was carried out as previously described (Liebau et al., 2009).

2.2. Crystallization

Crystallization of the wild type *Pf*GST in the tetrameric state (*Pf*GST^{apo}) was performed using the hanging-drop vapor-diffusion method. Hanging droplets were prepared by mixing 2 µl of the protein solution at a concentration of 18 mg/ml together with 2 µl of precipitating solution (2.1 M ammonium sulfate, 100 mM MES pH 6.0) and 0.5 µl of a seed stock (1:1000 diluted), containing micro-seed crystals. The preparation of the seed stock is described below.

The setups to grow the active form in complex with GSH (*Pf*GST^{GSH}) were performed and stored under an oxygen free environment using phosphate buffer instead of MES buffer (2.1 M ammonium sulfate, 100 mM phosphate buffer pH 6.5). Crystals appeared after 1 week at 20 °C with maximum seize of 500 µm.

Crystallization of the *Pf*GST$^{\Delta 114–118}$ was performed using the same method with the following modifications: Hanging droplets were made by mixing 3 µl of the protein solution with a concentration of 10 mg/ml with 3 µl of precipitating solution (2.3 M ammonium sulfate, 100 mM Tris/HCl pH 8.5). Droplets were equilibrated against 1 ml of precipitating solution. The crystallization trials were kept for about 1 week at 20 °C.

2.3. Preparation of a micro-seed-stock

Microgravity experiments were performed in terms of the DLR SIMBOX experiment (Preu and Braun, 2014) onboard of the chinese space mission Shenzhou8 (30.10.2011–17.11.2011). The SIMBOX counter diffusion crystallization experiments were coordinated by the Institute of Biophysics of the Chinese Academy of Sciences, Beijing. Prior to the microgravity experiments, crystallization conditions applying the compact counter diffusion flight hardware were extensively optimized under laboratory conditions, including transport simulations. The final protein solutions were analyzed by dynamic light scattering and showed a stable monodisperse peak for several days. The capillary length of the SIMBOX crystallization hardware was 10 mm with an inner diameter of 1 mm. The capillary was filled with a *Pf*GST solution using a concentration of 18 mg/ml and 2 % (w/v) low melting point agarose (Serva) was used to seal the capillaries. Subsequently, the capillaries were inserted carefully into a plastic casing, containing four separated sections filled with foam material and sealed with a metal lid. The foam was saturated with approximately 300 µl of precipitant solution (2.3 M ammonium sulfate, 100 mM Tris/HCl pH 8.5). For the microgravity experiment 4 capillaries were positioned in the DLR SIMBOX. The microgravity experiment was performed at a stable temperature of 20 °C for 17 days (30.10.2011–17.11.2011) onboard the Shenzou8 space mission. Following the space mission the capillaries were inspected directly after arrival in Beijing. The capillaries were opened at one end and the agarose was carefully removed. The obtained micro-crystals were used to prepare seed-stock solutions following the manufacturer's instructions of Jena BioScience Beads-for-Seeds.

2.4. Data collection and structure determination

Before data collection the crystals were soaked in the precipitating solution supplemented with 10% (v/v) glycerol for stabilization of the crystals during the freezing process. Diffraction data of *Pf*GST^{apo} were collected at 100 K at the P14 beamline at a wavelength of 1.24 Å (Petra III, EMBL-Hamburg, Germany) using a PILATUS 6 M detector. Data to 1.7 Å resolution were indexed, integrated, and scaled using XDS (Kabsch). The obtained crystals belong to the orthorhombic space group $P2_12_12$ with cell dimensions of $a = 86.4$, $b = 60.9$, $c = 74.8$ Å.

Diffraction data of wild-type *Pf*GST in the dimeric and active state in complex with GSH (*Pf*GST^{GSH}) were collected at 100 K at the consortiums beamline X13 (DORIS/DESY) on a MAR CCD detector at a wavelength of 0.804 Å. Data to 2.4 Å were indexed, integrated, and scaled by using HKL2000 (Otwinowski and Minor, 1997). The space group and unit cell parameters were assigned to the space group $P2_12_12_1$ with unit cell dimensions of $a = 57.4$, $b = 68.4$, $c = 122.7$ Å.

Diffraction data of the *Pf*GST$^{\Delta 114–118}$ were collected at 100 K at the consortiums beamline X13 (EMBL-Hamburg/DESY) at a wavelength of 0.804 Å using a MAR CCD detector. Data to 1.9 Å were indexed, integrated, and scaled by using HKL2000 (Otwinowski and Minor, 1997). Crystals belong to the same space group $P2_12_12$ with almost the identical cell dimensions to the wild-type enzyme in its tetrameric state.

For all datasets the asymmetric unit contains two monomers. The structures were determined by molecular replacement, using the program package MOLREP (CCP4, 1994) and the *Pf*GST structure (PDB code: 1PA3). The structure was carefully built using a bootstrapping procedure involving multiple model building rounds interspersed using maximum likelihood refinement in REFMAC5 (Murshudov et al., 1999) and the progress was monitored by a continuous decrease of the free *R*-value (Brunger, 1993). The CCP4 program suite (CCP4, 1994) and the program COOT (CCP4, 1994) were used for calculations and model building, respectively. Solvent molecules were automatically added at the end of the refinement process using the program wARP (Perrakis et al., 1999) and checked to confirm chemically reasonable positions where difference electron density exceeded a 3 σ level.

For all three structures the final electron density maps were of very good quality and the models indicated good stereochemistry. The quality of the final model was assessed by PROCHECK (Laskowski et al., 1993). The data collection and refinements statistics are summarized in Table 1. The coordinates for the structures, as well as the experimental diffraction amplitudes have been deposited at the Protein Databank (http://www.rcsb.org) with entry codes 3FR3, 3FR9 and 4ZXG. The protein interfaces and the protein ligand interactions were analyzed in detail using PDBsum (Laskowski et al., 1997) and LigPlot (Wallace et al., 1995).

2.5. Near UV measurements using CD spectroscopy

CD spectra in the near UV region were recorded on a JASCO J-815 spectrometer (JASCO, Easton, USA). Experiments were implemented at wavelengths between 340 and 240 nm using a 1.0 cm quartz cuvette; the protein concentration was 4 mg/ml. All data were obtained from two independent experiments. For each experiment the protein measurements were repeated 15 times, the blank (buffer) measurements were repeated 5 times. Subtraction of the buffer data from the protein data resulted in a clear CD spectra. By conducting near UV experiments in 20 mM K_2HPO_4, 100 mM MES, pH 7.5, the *Pf*GST binding of MES was analyzed in solution. Control-measurements were done in absence of MES.

The CD spectra (±MES) were compared and analyzed by superposition to follow the decrease in the appropriate spectra of the

Table 1
Data collection and refinement statistics.

	*Pf*GST^{apo}	*Pf*GST^{GSH}	*Pf*GST$^{\Delta 114–118 + GSSG}$
Space group	$P2_12_12$	$P2_12_12_1$	$P2_12_12$
a (Å)	60.9	57.4	60.9
b (Å)	86.4	68.4	87.1
c (Å)	74.8	122.7	74.8
V_M (Å^3/Da)	2.0	2.4	2.0
Solvent content (%)	38.0	49.3	39.7
Resolution (Å)	30–1.7 (1.7–1.75)	20–2.4 (2.4–2.46)	20–1.9 (1.9–1.95)
No. of total refections	273,546	128,383	235,301
Redundancy	6.2	7.1	7.9
Completeness of data (%)	98.3 (78.2)	97.2 (94.0)	98.6 (98.0)
Average *I*/sigma Intensity	30.5 (3.6)	14.3 (2.9)	20.1 (3.6)
No. of reflections used in refinement	43,889	17,966	29,646
R_{merge} (%)[a]	2.6 (42.1)	8.6 (44.6)	8.6 (54.2)
R_{work} (%)[b]	18.3 (25.6)	24.3 (26.9)	21.1 (25.0)
R_{free} (%)[c]	22.9 (30.8)	29.6 (31.4)	25.2 (34.9)
Protein atoms	3718	3308	3261
Solvent atoms	218	122	212
Ligand atoms	56	40	80
Mean *B* value (Å^2)	21.9	26.7	33.9
Root mean square deviation			
Bonds (Å)	0.02	0.006	0.02
Bond angels (°)	1.7	0.89	1.9

[a] R_{merge} is defined as $\sum_{hkl}\sum_i |I_i(hkl) - [I(hkl)]|/\sum_{hkl}\sum_i I_i(hkl)$, where I_i(hkl) is the intensity of an individual measurement and [I(hkl)] is the mean intensity from multiple observations of this reflection.

[b] $R_{work} = \sum||F_{obs}| - |F_{calc}||/\sum|F_{obs}|$, where F_{obs} and F_{calc} are observed and calculated structure factors.

[c] R_{free} was calculated using a randomly selected 5% of the reflections.

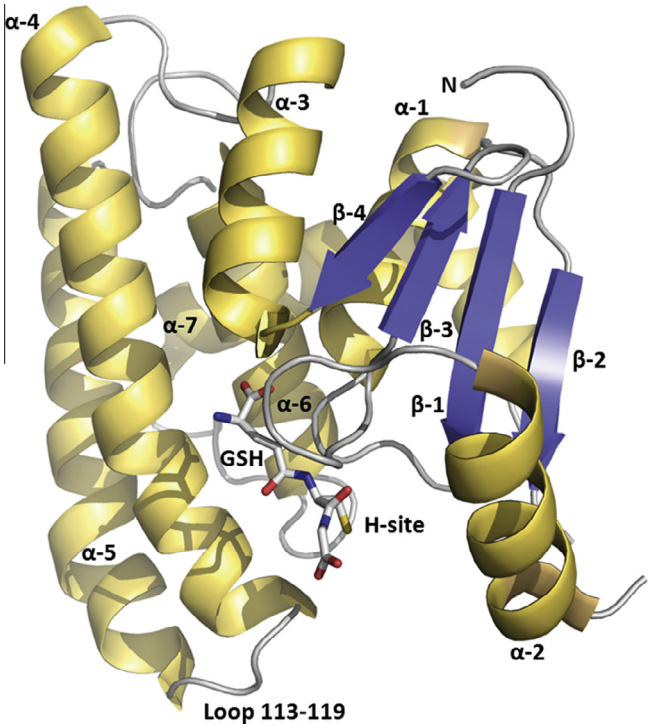

Fig. 1. The *Pf*GST monomer, emphasizing the secondary structure elements. Helices are colored yellow, β-strands are colored blue. *Pf*GST is composed out of two domains. The first domain consists of four β-sheets with three flanking α-helices. Domain 2 is built up entirely from five α-helical segments connected by a variety of loops. The GSH molecule bound to the G-site is shown in stick representation. The H-site is located next to the G-site flanked by the C-terminal part of β-sheet β1 and β2 and the N-terminal part of helix α1. Loop 113–119 connects helix α4 and α5.

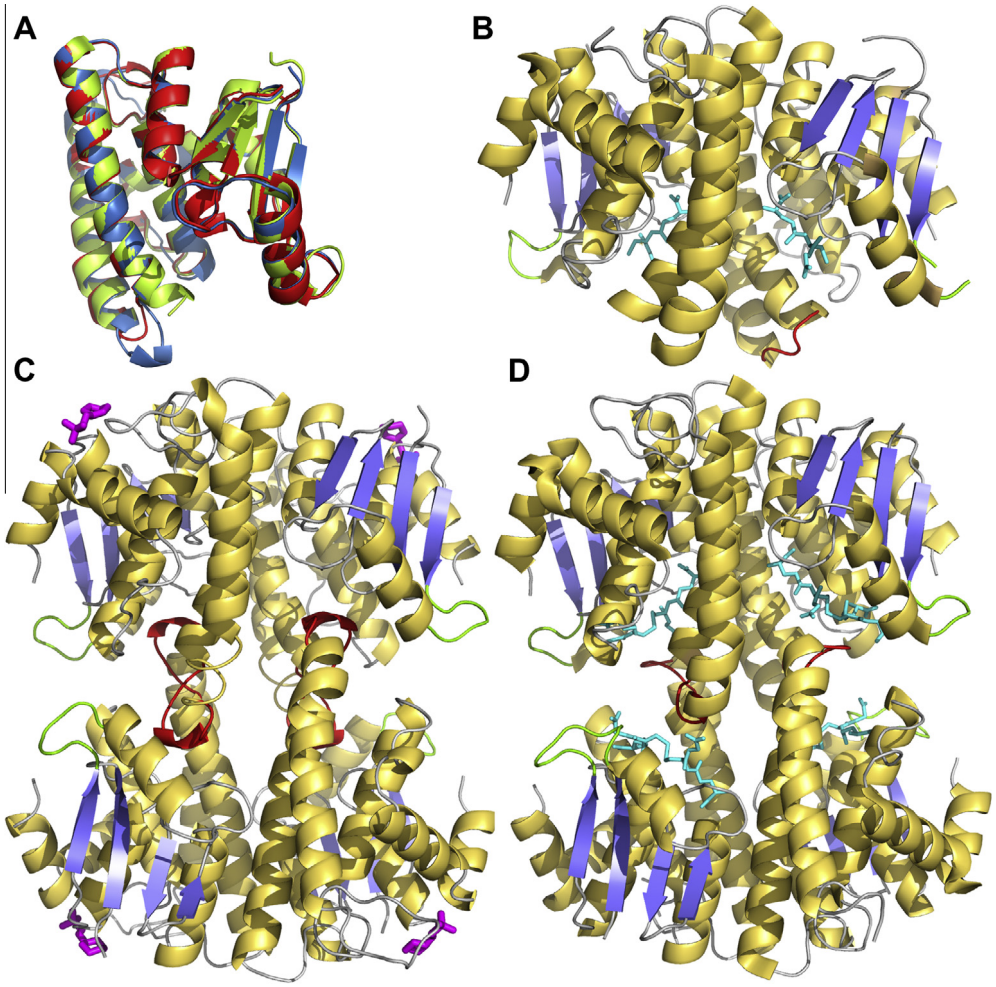

Fig. 2. (A) The superposition of monomers forming active dimers (shown in B) or inactive tetramers (shown in C and D) reveal no significant changes of the overall fold. (B) Wild-type *Pf*GST is able to form active dimers. In the active form GSH is bound to the active site. Two bound GSH molecules are shown in stick representation and colored in cyan. The characteristic Mu-loop, located between β-sheet 2 and α-helix 2 is colored in green and loop 113–119 is colored in red. (C) Two active dimers form the enzymatically inactive tetramer. The inactive tetramers are not able to bind GSH. Four bound MES molecules are shown in stick representation and colored in magenta. The Mu-loop and loop 113–119 are colored as in (B). (C) *Pf*GST$^{\Delta 114-118}$ that is missing major parts of loop 113–119 is also able to form stable tetramers. Moreover four GSSG molecules, shown in stick representation and colored in cyan, bind tightly to all G-sites.

aromatic amino acids and to identify the interaction between proteins and MES molecules in solution. Results are expressed as molar ellipticity $[\theta]$ (deg cm^2 dmol^{-1}), calculated from the following equation $[\theta] = \theta/10 * c * l * n_r$, where θ is the measured ellipticity in millidegree, c is the protein concentration in molar units, l the light path length in cm, and n_r is the number of the residues. The overall mean value for the experimental error of the molar ellipticity $[\theta]$ was 0.5 and 0.4 (±MES). All data points presented in Fig. 7 are expressed as mean ± standard deviation (SD), according to the following Eq. (1).

$$s = \sqrt{\frac{1}{N-1}\sum_{i=1}^{N}(x_i - \bar{x})^2} \quad (1)$$

3. Results and discussion

3.1. Overall structures of wild-type PfGST in the dimeric and tetrameric state

For the first time we have crystallized the enzymatically active form in complex with reduced GSH in the dimeric state. The structure was refined to a resolution of 2.4 Å. The overall structure of the monomers (Fig. 1) coincides with previously reported *Pf*GST structures (Fritz-Wolf et al., 2003; Hiller et al., 2006; Perbandt et al., 2004). A functional active homodimer (Fig. 2) forms the asymmetric unit (Fig. 3A). The overall fold of the monomers within the asymmetric unit is very similar and can be superimposed with an r.m.s deviation of less than 0.5 Å for all C-alpha positions (Fig. 2A). The space group and unit cell axis differ in comparison to the tetrameric state, even if the crystallization conditions are quite comparable (Table 1).

The intermolecular interactions at the subunit interface of the active dimers are characterized by several hydrophilic interactions (Table 2). Particularly, the side chain of Arg77 serves as a hydrophilic anchor and forms two hydrogen bridges to the side chain of Asp97 from the other subunit of the homodimer. This arginine-mediated intersubunit contact is class-specific for Mu-class GSTs (Dirr et al., 1994). Besides this specific feature, hydrophobic interactions are the dominating force of the dimerization. These "lock and key" motifs are common for several GST-classes and offer a good possibility to distinguish between the classes (Sinning et al., 1993). Here Phe56 acts as the "key", which fits into the hydrophobic "lock" formed by Trp131, Phe135

and Tyr134 of the other subunit. This structural feature is also unique for Mu-class GSTs. Active dimers (Fig. 2B) reveal an interaction interface of 1.347 Å^2, corresponding to 12% of the total monomer surface of 11.489 Å^2.

The inactive tetrameric state (Fig. 2C) of the wild-type *Pf*GST was determined at a resolution of 1.7 Å. Here again a dimer forms the asymmetric unit. However these dimers do not match to the active homodimers. Therefore they are named non-active dimers. The inactive tetramer is formed by a crystallographic 2-fold axis from two non-active dimers (Fig. 3B). The non-active dimers show an interaction interface of 1.121 Å^2, corresponding to 9.7% of the total monomer surface. The interface is stabilized by hydrogen bonds, but dominated by hydrophobic interactions. The intersubunit interactions are summarized in Table 3. Particular residues located within loop 113–119 are involved in these direct hydrogen bonds and further mediate almost all of the hydrophobic interactions. In the tetrameric state two homodimers are interlocked with each other by loop 113–119 and form the tetramer. The active site is blocked by loop 113–119 and therefore the tetrameric state remains enzymatically inactive.

Table 2
Characteristic direct intersubunit interactions at the interface of the active dimer in *Pf*GST^{apo}, *Pf*GST^{GSH} and *Pf*GST$^{\Delta 114-118}$.

Residue subunit 1	Residue subunit 2
Hydrogen bonds	
Glu^{57} OE1^{Acc}	Tyr^{134} OH^{Don}
Arg^{77} NE^{Don}	Asp^{97} OD2^{Acc}
Arg^{77} NH2^{Don}	Asp^{97} OD1^{Acc}
Tyr^{134} OH^{Don}	Glu^{57} OE1^{Acc}
Asp^{97} OD2^{Acc}	Arg^{77} NE^{Don}
Asp^{97} OD1^{Acc}	Arg^{77} NH2^{Don}
Hydrophobic interactions	
Phe^{56}	Trp^{131}, Tyr^{134}, Phe^{135}
Trp^{131}, Tyr^{134}, Phe^{135}	Phe^{56}

Interestingly, for the inactive tetrameric state we identified a ligand-binding site occupied by one MES molecule in each of the four monomers. This novel non-substrate binding site will be described later.

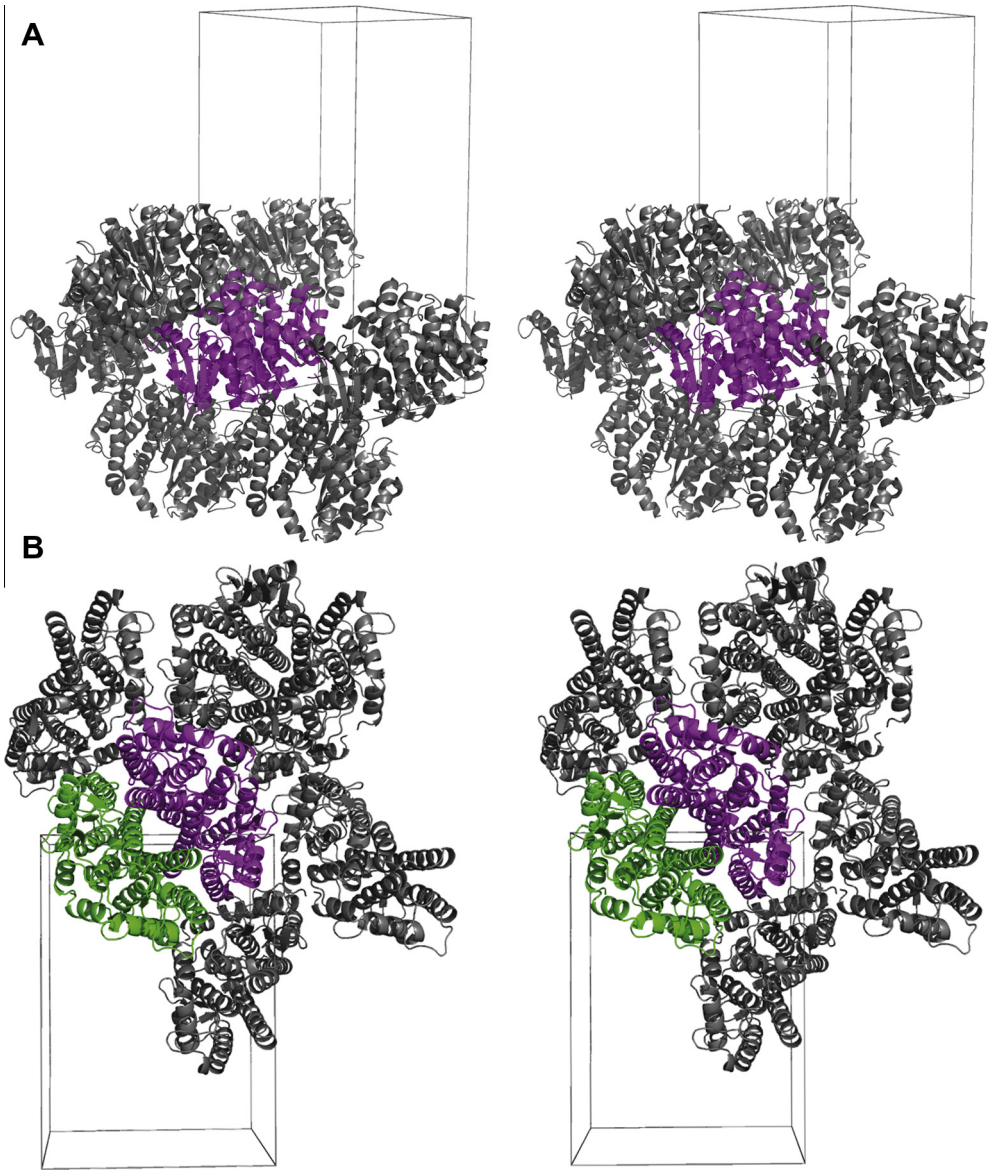

Fig. 3. A stereo view towards the crystal packing of the *Pf*GST in the active dimeric form (A) and inactive tetrameric form (B). Both states are crystallized in different space groups. Crystals of the active dimers belong to space group $P2_12_12_1$ and crystals of the inactive tetramers to space group $P2_12_12$. Molecules in the asymmetric unit are colored in magenta. The inactive tetramer is formed by a crystallographic 2-fold axis along the *c*-axis. The crystal lattice in (A) allows no formations of tetramers.

Table 3
Characteristic direct intersubunit interactions at the interface of the tetrameric structures of *Pf*GST^{apo} and *Pf*GST$^{\Delta 114-118}$.

*Pf*GST^{apo}		*Pf*GST$^{\Delta 114-118}$	
Residue subunit 1	Residue subunit 2	Residue subunit 1	Residue subunit 2
Hydrogen bonds			
Asn^{111} O^{Acc}	Asn^{114} ND2^{Don}	None	None
Asn^{112} OD1^{Acc}	Lys^{117} NZ^{Don}		
Asn^{114} ND2^{Don}	Asn^{111} O^{Acc}		
Lys^{117} NZ^{Don}	Asn^{112} OD1^{Acc}		
Hydrophobic interactions			
Phe^{10}, Phe^{42}, Phe^{45}	Leu^{124}, Tyr^{176}	Phe^{10}, Phe^{42}, Phe^{45}	Leu^{124}, Tyr^{176}
Tyr^{9}, Phe^{10}, Ala^{12}	Leu^{115}	Leu^{124}, Tyr^{176}	Phe^{10}, Phe^{42}, Phe^{45}
Lys^{15}, His^{107}, Tyr^{108}	Phe^{116}		
Gln^{58}, Val^{59}	Gln^{118}		
Asn^{111}	Asn^{114}, Phe^{116}		
Leu^{124}, Tyr^{176}	Phe^{10}, Phe^{42}, Phe^{45}		
Leu^{115}	Tyr^{9}, Phe^{10}, Ala^{12}		
Phe^{116}	Lys^{15}, His^{107}, Tyr^{108}		
Gln^{118}	Gln^{58}, Val^{59}		
Asn^{114}, Phe^{116}	Asn^{111}		

Residues that are part of Loop$^{113-119}$ are underlined.

3.2. Structural characteristics of the G-site and H-site

The comparison of *Pf*GST with the human Mu-class enzyme (Raghunathan et al., 1994) revealed a sequence identity of 24% with an r.m.s. deviation of 2.6 Å for Cα-atoms. The highest differences are in the regions of the Mu-loop, the C-terminal tail, and loop 113–119 formed by helix α4 and helix α5 (Figs. 1 and 2). The sequence comparison of *Pf*GST with GSTs from other organisms revealed a rather low sequence similarity. The highest sequence identity is observed with the GST from *Wuchereria bancrofti* GST (PDB entry code 3T2U, to be published) with only 31%.

As previously reported in detail by us (Perbandt et al., 2004), in typical Mu-class GSTs, the Mu-loop and C terminus are connected by interchain hydrogen bonds and form a characteristic deep cleft shielding the G- and H-sites from one side. However, since the G- and H-sites of the *Pf*GST are not shielded by the Mu-loop and the C terminus they are much more exposed to the solvent (Fig. 4). The additional space between the Mu-loop and the C terminus found in the plasmodial enzyme may support the design of parasite-specific synthetic inhibitors. Although the G-site of *Pf*GST and mammalian Mu-class GSTs is structurally similar, the H-site of the GSTs differs significantly. The most significant difference is the replacement of the typical Mu-loop by a short turn in *Pf*GST. This structural feature is also described for the GST from *Schistosoma japonicum*, a trematode that causes schistosomiasis (Cardoso et al., 2003). A further comparison of the H-site from *Pf*GST with that of other GST classes indicates a higher similarity to a typical Pi-class enzyme. In principle, the G- and the H-sites of *Pf*GST combine structural features of the Pi- and the Mu- classes. Therefore, we can consider the *Pf*GST as a "chimeric enzyme." This general conclusion is supported by the biochemical characterization of the enzyme (Harwaldt et al., 2002; Liebau et al., 2002).

The comparison of the wild-type *Pf*GST in an inactive tetrameric state, the wild-type *Pf*GST in a dimeric state and the loop mutant form in a tetrameric state reveal no significant structural differences or conformational changes for the G- and H-site. The binding sites are rigid and not changed by the dimer–tetramer transition. The superposition of the monomers in the dimeric and tetrameric state shows a low r.m.s. deviations of 0.38 Å (for *Pf*GST^{GSH} and *Pf*GST^{apo}) and 0.51 Å (for *Pf*GST^{GSH} and P*f*GST$^{\Delta 114-118}$) for all corresponding C-alpha positions.

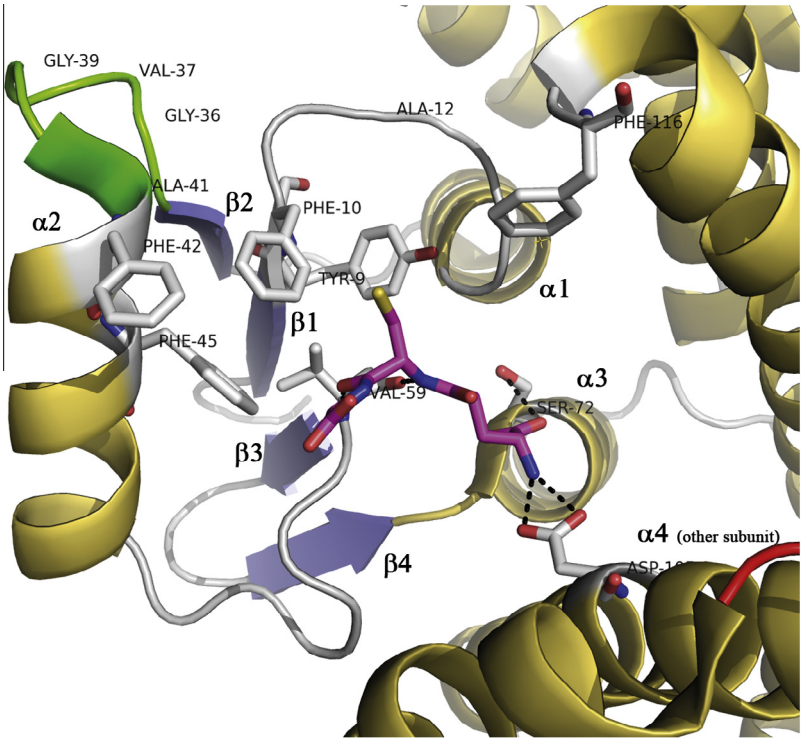

Fig. 4. View to the G-site and H-site with bound GSH to the G-site. GSH is bound by direct hydrogen bridges from Ser72 and Val59 and Asp105 (from subunit B of the active dimer). The electrophilic H-site is dominated by hydrophobic residues (Tyr9, Phe10, Phe42, and Phe45) and flanked by the Mu-loop (colored in green).

3.3. The quaternary structure of $PfGST^{\Delta 114-118}$

Since a structural knowledge about the dimer–tetramer transition is important to develop new potential inhibitors and since we are interested to elucidate the structural basis of this observation, we carried out an X-ray crystallographic analysis of a mutant with a truncated loop region. The loop region 114–118 (Asn^{114}, Leu^{115}, Phe^{116}, Lys^{117} and Glu^{118}) was replaced by two alanine residues.

We expected that the modification of $loop^{113-119}$ stabilizes the dimer species as indicated by the recent kinetic data (Liebau et al., 2009) and the aim was to crystallize the active dimer in complex with reduced GSH.

Surprisingly, our X-ray structural analysis revealed the opposite. The obtained structure of $PfGST^{\Delta 114-118}$ at 1.9 Å resolution resembles a consistent tetrameric architecture as observed for the wild-type *Pf*GST in the inactive, GSH-free state (Fig. 2D). Accordingly, the intermolecular interactions at the subunit interface of the active dimer of $PfGST^{\Delta 114-118}$ are preserved in comparison to the wild-type *Pf*GST in the inactive, GSH-free state (Table 2). This results in an almost identical interaction interface of 1.350 $Å^2$

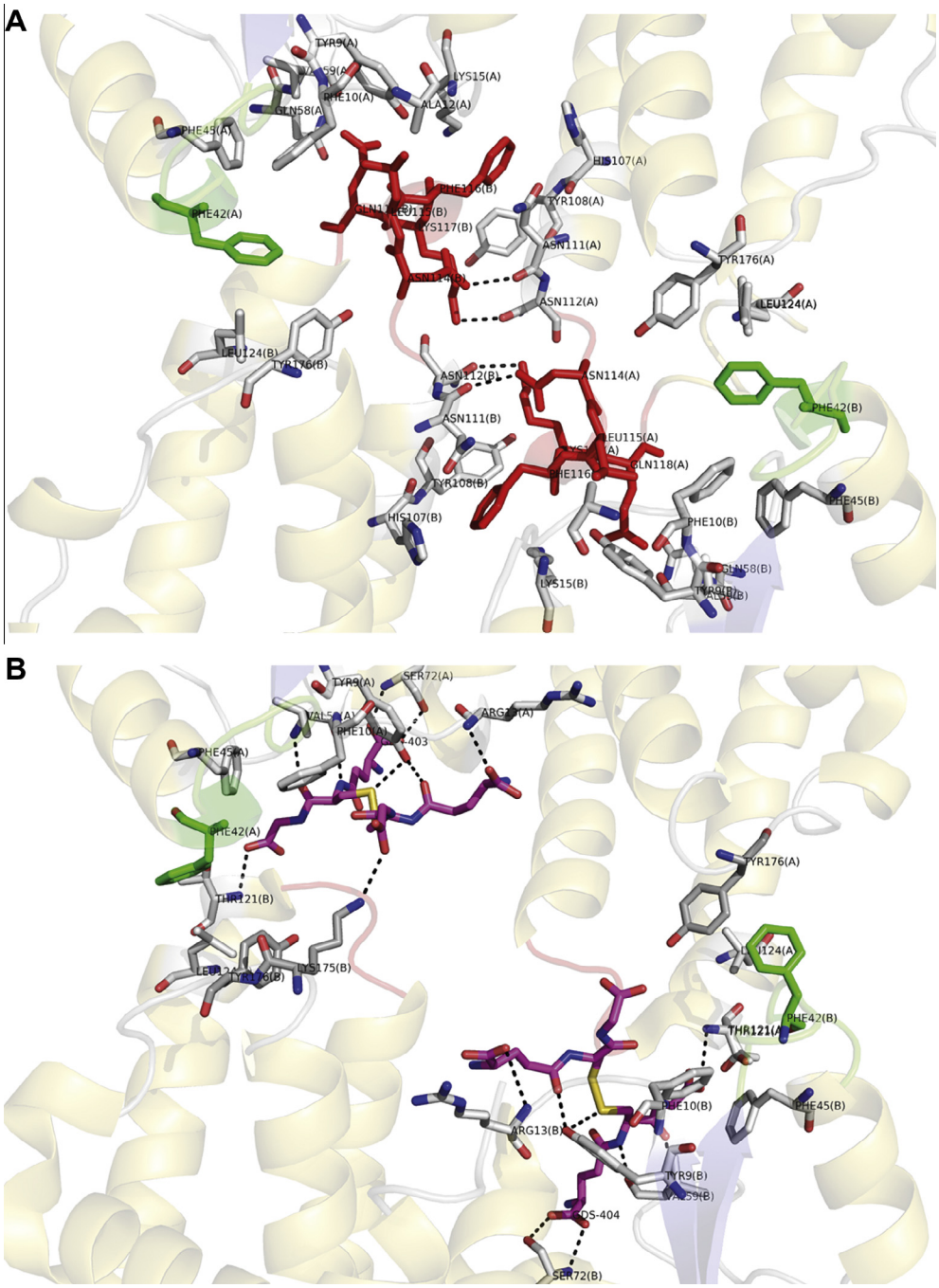

Fig. 5. (A) A close up view to the interface region between two dimers forming the tetramer in wild-type *Pf*GST. The loop region 113–119 is colored in red. The loop stabilizes the tetramer by several direct hydrogen bonds to residues of the other subunit. All other residues shown in stick representation are involved in hydrophobic interactions. Phe42 of the Mu-loop is colored in green. (B) A close up view to the corresponding region of $PfGST^{\Delta 114-118}$. GSSG is bound to the active site and stabilized by direct hydrogen bonds hydrophobic interactions. The number of intersubunit interactions is significantly reduced compared to the wild-type tetramer. The comparison between (A) and (B) reveals that $loop^{113-119}$ occupies most of the G-site of the neighboring molecule and blocks the binding of the substrate to the active site. Significantly more space is available for the truncated loop in $PfGST^{\Delta 114-118}$, also enabling the binding of GSSG in the tetrameric state.

corresponding to 13% of the total monomer surface of 10,690 Å^2. Moreover, all G-sites and parts of the H-sites are occupied by oxidized glutathione (GSSG) instead of reduced glutathione (GSH).

In one of our previous studies we found that GSSG prevents the inactivation process, thus stabilizing the dimeric structure of the wild-type enzyme and behaving like an unambiguous competitive inhibitor (Liebau et al., 2009). Furthermore, another group reported that the interaction between Asn112 and Lys117 from neighboring subunits is most essential to keep the tetramer structure stable (Quesada-Soriano et al., 2014).

However, the data we summarize here show that loop$^{113–119}$ is not required to form stable tetramers and GSSG is not preventing the tetramerization process for *Pf*GST$^{\Delta 114–118}$ at high protein concentrations. At lower concentrations the interactions through the loop can influence the oligomerization kinetics as reported by us previously (Liebau et al., 2009). Neither the wild-type *Pf*GST nor

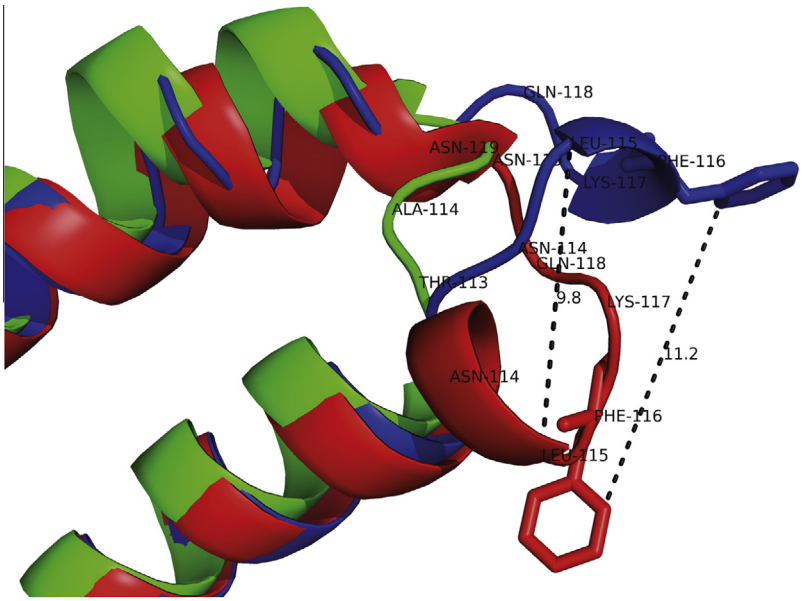

Fig. 6. The conformation of loop 113–119 differs significantly for the active dimer with bound GSH (red) compared with the inactive tetramer (blue). Corresponding atom positions of Phe116 reveal a maximal displacement of more than 10 Å. The conformation of the truncated loop in *Pf*GST$^{\Delta 114–118}$ is shown in green.

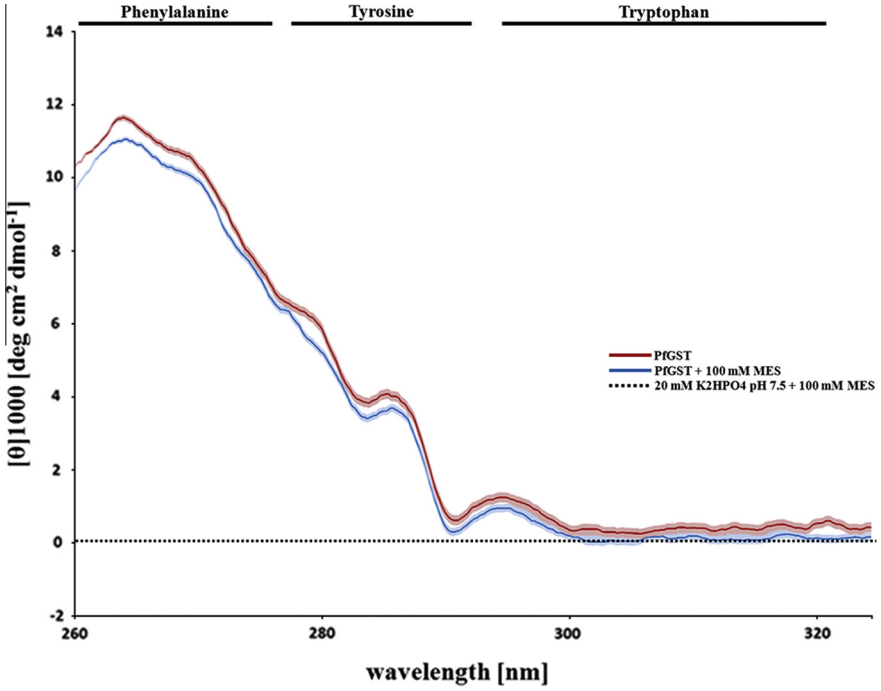

Fig. 7. The near UV spectrum of the *Pf*GST with 100 mM MES (blue) shows a decrease in the tyrosine (275–290 nm) and phenylalanine (260–275 nm) region compared to the defined near UV spectrum of the *Pf*GST (red), while the tryptophan region (290–320 nm) remains unaffected. The corridor (in light blue and light red) represents the standard deviation of the data points.

*Pf*GST$^{\Delta 114-118}$ have been purified or crystallized in presence of any phosphate ions. Therefore we cannot support the formerly made hypothesis that the formation of tetramers is caused by a phosphate- or pyrophosphate-induced process (Quesada-Soriano et al., 2014).

Our data may also explain why the tetramerization in absence of GSH is 100 times slower for *Pf*GST$^{\Delta 114-118}$ than observed for the wild-type enzyme (Liebau et al., 2009). The interface between two active dimers forming the tetramer of *Pf*GST$^{\Delta 114-118}$ differs significantly in comparison to the tetrameric state of the wild-type *Pf*GST (Fig. 5). The truncation of loop$^{113-119}$ results in a drastic reduction of direct intramolecular interactions within the tetramer (see Table 3). For the *Pf*GST$^{\Delta 114-118}$ tetramer the surface area between the non-active dimers covers only 331 Å^2 in comparison to 1.121 Å^2 for the wild-type enzyme. No direct hydrogen bonds are formed between the subunits (Table 3), and the hydrophobic interactions are mediated by residues Phe10, Phe42 and Phe45 from the first subunit and Leu124 and Tyr176 from the corresponding subunit (Fig. 5B).

Remarkably, Phe42 and Phe45 are part of, or flank the most characteristic Mu-loop (Fig. 4), which is located between β-sheet 2 and α-helix 2 (Ji et al., 1992). For *Pf*GST, the Mu-loop is formed by residues 35–42 and is significantly smaller in comparison with more typical Mu-class GSTs. The side chains of the Mu-loop form part of the electrophilic substrate-binding H-site. Only the truncated Mu-loop in *Pf*GST enables the formation of the tetrameric inactive complex. An extended loop would probably sterically interfere with the tetramer-complex formation. One can propose that the replacement of the typical Mu-loop by a short turn in *Pf*GST is an evolutionary development to enable the unique dimer–tetramer transition observed for *Pf*GST.

For *Pf*GST$^{\Delta 114-118}$ the substantial reduction of direct interactions is mainly caused by the truncated loop$^{113-119}$ (Fig. 2). For the wild-type *Pf*GST the intact loop mediates the majority of hydrophobic interactions between the subunits (Fig. 5 and Table 3). However the reduced number of interactions is partially compensated by GSSG-mediated interactions between the subunits. Expectably, GSSG is tightly bound by hydrogen bonds and hydrophobic interactions mediated by G-site residues of one subunit (Fig. 3). Additional hydrogen bonds formed by Thr121 and Lys175 from the other subunit stabilize the tetrameric state. In summary one can postulate that in tetramer formation GSSG has the effect of an adhesive.

We can assume that the oxidation of GSH to GSSG facilitates the tetramerization of the mutant. Further, only the truncated loop provides sufficient space to allow GSSG binding in the tetrameric state. The direct structural comparison (Fig. 5) of a tetramer of the mutant with the tetramer of the wild-type enzyme reveals that GSH or other specific ligands are not able to bind to tetramers of the wild-type enzyme, because amino acids of loop$^{113-119}$ occupy major parts of the G-site as well as H-site in the neighboring molecule.

The comparison of all three structures (*Pf*GST^{apo}, *Pf*GST^{GSH} and *Pf*GST$^{\Delta 114-118}$ reveals that loop 113–119 exhibit different conformations in the active dimeric state to the inactive tetrameric state (Fig. 6). This observation is in good agreement with other structures already deposited in the Protein Data Bank (PDB entry codes 2AAW and 1OKT). Since major parts of the loop are missing in *Pf*GST$^{\Delta 114-118}$ but nevertheless stable tetramers are formed, we conclude that conformational changes in the loop region$^{113-119}$ are the effect but not the reason of tetramerization.

In summary, it is obvious that inhibitors tightly bound to the *Pf*GST will prevent the dimer–tetramer transition due to sterical hindrance and inhibitor binding to the G- or H-site and tetramerization are therefore competitive processes.

3.4. Identification of a non-substrate-binding pocket

Surprisingly the obtained wild-type *Pf*GST structure determined at a resolution of 1.7 Å clearly revealed a non-substrate binding

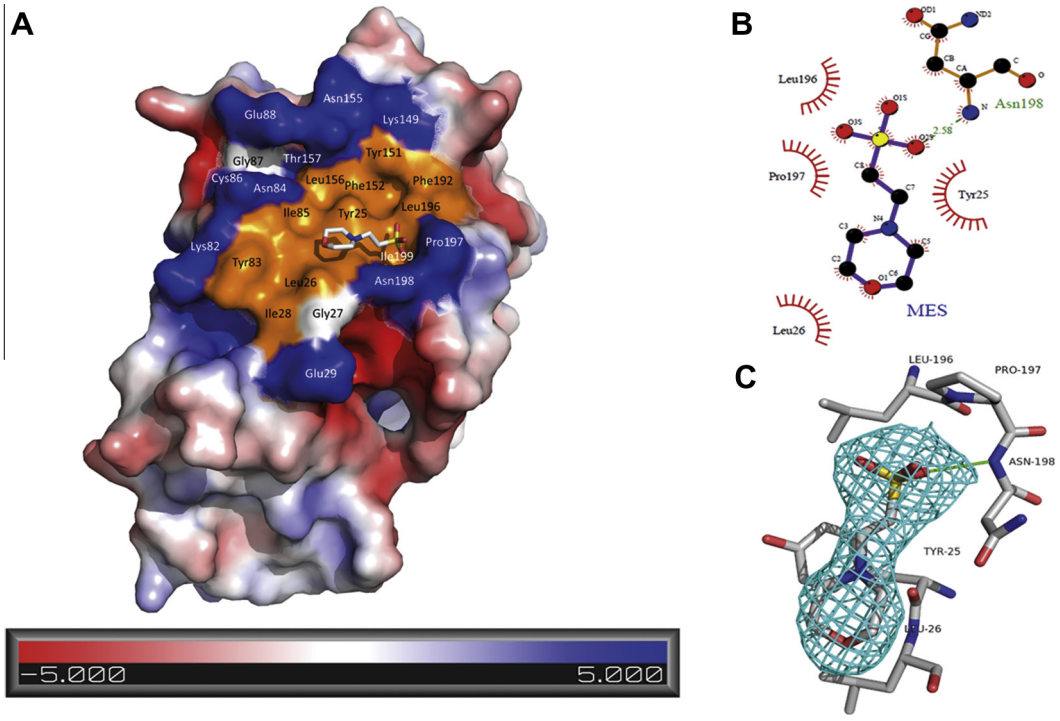

Fig. 8. (A) Non-substrate-binding site and hydrophobic cleft of *Pf*GST with bound MES. Hydrophobic residues are colored in orange and hydrophobic residues in blue. The remaining surface is shown according to the electrostatic potential charge. (B) Schematic drawing of bound MES to *Pf*GST. Hydrophobic interactions are mediated by residues Tyr25, Leu26, Leu196, Pro197. Asn198 mediates a hydrogen bridge to the MES molecule. The drawing was made using the program LigPlot (Wallace et al., 1995). (C) MES superimposed on a $F_o - F_c$ difference electron density map, countered at 2.5 σ, indicating that it is tightly bound within the binding pocket.

pocket occupied by a MES molecule for all monomers. The localization of ligand-binding-sites for several classes of GSTs is controversially discussed and remains unclear and inconsistent (Axarli et al., 2004; Ji et al., 1996; McTigue et al., 1995; Oakley et al., 1999).

The specific binding of the MES molecule to GSTs in solution was further analyzed by spectroscopic fluorescence methods (Prade et al., 1997). Indeed, the near UV measurements by CD spectroscopy showed a decreased absorbance in the tyrosine and phenylalanine spectra compared to a defined near UV spectrum of the *Pf*GST without MES (Fig. 7). *Pf*GST altogether possesses 16 tyrosine residues, but the crystal structure reveals that only Tyr25 is shielded by the MES molecule. This circumstance explains the weak difference of the absorbance in the near UV spectra. Therefore, the solution experiments are in good agreement with the results of the crystallographic analysis.

The binding pocket is formed by the residues Tyr25, Leu26, Leu196, Pro197 and Asn198. The binding mode of the MES molecules is particular stabilized by a hydrogen bond mediated by the amide nitrogen from Asn198 (Fig. 8). For *Pf*GST the region around the amino acids Leu196, Pro197, Asn198 and Ile199 is strongly positively charged. The negatively charged ethane sulfonic moiety of the MES molecule forms a hydrogen bond to Asn198. Additional hydrophobic interactions are mediated by Leu26, Leu196, Pro197 and Tyr25.

The novel L-site is part of the outer end of a large hydrophobic groove, spanning transversely through the surface of the *Pf*GST monomer (Fig. 8). This hydrophobic groove is composed of 11 hydrophobic residues and flanked by 10 hydrophilic residues and extends to about 20 Å and a width of 12 Å. This accessible mainly hydrophobic groove is also present in *Pf*GST$^{\Delta 114-118}$.

4. Conclusions

The high resolution structural analysis of *Pf*GST$^{\Delta 114-118}$ in complex with GSSG clearly showed that loop 113–119 is not essential to form stable tetramers as reported before. The loop region 114–118 (Asn^{114}, Leu^{115}, Phe^{116}, Lys^{117} and Glu^{118}) was replaced and shortened by two alanine residues (*Pf*GST$^{\Delta 114-118}$). The structural data shown here indicate that the loop reduction can be partially compensated by GSSG mediated interactions between the subunits. In summary, GSSG has an adhesive effect and supports the tetramer formation. Evidently conformational changes of the loop region are not the reason but the cause of the tetramerization. The binding of ligands to the G- or H-site and the dimer–tetramer transition seem to be competitive processes. Furthermore, we identified a novel non-substrate-binding site of the wild-type *Pf*GST structure in complex with 2-(N-morpholino) ethanesulfonic acid (MES). The localization of ligandin-binding-sites is still controversially discussed and remains unclear and inconsistent. The identified binding site reveals new structural information about the so far unexploited *Pf*GST L-site.

Acknowledgements

This work was supported by grants from the Deutsche Forschungsgemeinschaft (German-African Cooperation Projects in Infectiology-PAK296), by the excellence cluster 'The Hamburg Centre for Ultrafast Imaging – Structure, Dynamics and Control of Matter at the Atomic Scale' of the Deutsche Forschungsgemeinschaft, by the Hamburg Ministry of Science and Research and Joachim Herz Stiftung as part of the Hamburg Initiative for Excellence in Research, the Hamburg School for Structure and Dynamics in Infection (SDI) and by DLR via grant 50WB1017.

References

Axarli, I.A., Rigden, D.J., Labrou, N.E., 2004. Characterization of the ligandin site of maize glutathione S-transferase I. Biochem. J. 382, 885–893.
Brunger, A.T., 1993. Assessment of phase accuracy by cross validation: the free *R* value. Methods and applications. Acta Crystallogr. D Biol. Crystallogr. 49, 24–36.
Burmeister, C., Perbandt, M., Betzel, C., Walter, R.D., Liebau, E., 2003. Crystallization and preliminary X-ray diffraction studies of the glutathione S-transferase from *Plasmodium falciparum*. Acta Crystallogr. D Biol. Crystallogr. 59, 1469–1471.
Cardoso, R.M., Daniels, D.S., Bruns, C.M., Tainer, J.A., 2003. Characterization of the electrophile binding site and substrate binding mode of the 26-kDa glutathione S-transferase from *Schistosoma japonicum*. Proteins 51, 137–146.
CCP4, 1994. The CCP4 suite: programs for protein crystallography. Acta Crystallogr. D Biol. Crystallogr. 50, 760–763.
Deponte, M., Becker, K., 2005. Glutathione S-transferase from malarial parasites: structural and functional aspects. Methods Enzymol. 401, 241–253.
Dirr, H., Reinemer, P., Huber, R., 1994. X-ray crystal structures of cytosolic glutathione S-transferases. Implications for protein architecture, substrate recognition and catalytic function. Eur. J. Biochem. 220, 645–661.
Fritz-Wolf, K., Becker, A., Rahlfs, S., Harwaldt, P., Schirmer, R.H., Kabsch, W., Becker, K., 2003. X-ray structure of glutathione S-transferase from the malarial parasite *Plasmodium falciparum*. Proc. Natl. Acad. Sci. U.S.A. 100, 13821–13826.
Frova, C., 2006. Glutathione transferases in the genomics era: new insights and perspectives. Biomol. Eng. 23, 149–169.
Greenwood, B., Mutabingwa, T., 2002. Malaria in 2002. Nature 415, 670–672.
Harwaldt, P., Rahlfs, S., Becker, K., 2002. Glutathione S-transferase of the malarial parasite *Plasmodium falciparum*: characterization of a potential drug target. Biol. Chem. 383, 821–830.
Hayes, J.D., Flanagan, J.U., Jowsey, I.R., 2005. Glutathione transferases. Annu. Rev. Pharmacol. Toxicol. 45, 51–88.
Hiller, N., Fritz-Wolf, K., Deponte, M., Wende, W., Zimmermann, H., Becker, K., 2006. Plasmodium falciparum glutathione S-transferase-structural and mechanistic studies on ligand binding and enzyme inhibition. Protein Sci. 15, 281–289.
Ji, X., Zhang, P., Armstrong, R.N., Gilliland, G.L., 1992. The three-dimensional structure of a glutathione S-transferase from the mu gene class. Structural analysis of the binary complex of isoenzyme 3-3 and glutathione at 2.2-A resolution. Biochemistry 31, 10169–10184.
Ji, X., von Rosenvinge, E.C., Johnson, W.W., Armstrong, R.N., Gilliland, G.L., 1996. Location of a potential transport binding site in a sigma class glutathione transferase by x-ray crystallography. Proc. Natl. Acad. Sci. U.S.A. 93, 8208–8213.
Kabsch, W., 0000. Acta Crystallogr. D Biol. Crystallogr. 66, 125–132.
Laskowski, R.A., MacArthur, M.W., Moss, D.S., Thornten, J.M., 1993. PROCHECK: a program to check the stereochemical quality of protein structures. J. Appl. Cryst. 26, 283–291.
Laskowski, R.A., Hutchinson, E.G., Michie, A.D., Wallace, A.C., Jones, M.L., Thornton, J.M., 1997. PDBsum: a Web-based database of summaries and analyses of all PDB structures. Trends Biochem. Sci. 22, 488–490.
Liebau, E., Bergmann, B., Campbell, A.M., Teesdale-Spittle, P., Brophy, P.M., Luersen, K., Walter, R.D., 2002. The glutathione S-transferase from *Plasmodium falciparum*. Mol. Biochem. Parasitol. 124, 85–90.
Liebau, E., De Maria, F., Burmeister, C., Perbandt, M., Turella, P., Antonini, G., Federici, G., Giansanti, F., Stella, L., Lo Bello, M., Caccuri, A.M., Ricci, G., 2005. Cooperativity and pseudo-cooperativity in the glutathione S-transferase from *Plasmodium falciparum*. J. Biol. Chem. 280, 26121–26128.
Liebau, E., Dawood, K.F., Fabrini, R., Fischer-Riepe, L., Perbandt, M., Stella, L., Pedersen, J.Z., Bocedi, A., Petrarca, P., Federici, G., Ricci, G., 2009. Tetramerization and cooperativity in *Plasmodium falciparum* glutathione S-transferase are mediated by atypic loop 113–119. J. Biol. Chem. 284, 22133–22139.
Mannervik, B., Danielson, U.H., 1988. Glutathione transferases–structure and catalytic activity. CRC Crit. Rev. Biochem. 23, 283–337.
McTigue, M.A., Williams, D.R., Tainer, J.A., 1995. Crystal structures of a schistosomal drug and vaccine target: glutathione S-transferase from *Schistosoma japonica* and its complex with the leading antischistosomal drug praziquantel. J. Mol. Biol. 246, 21–27.
Murshudov, G.N., Vagin, A.A., Lebedev, A., Wilson, K.S., Dodson, E.J., 1999. Efficient anisotropic refinement of macromolecular structures using FFT. Acta Crystallogr. D Biol. Crystallogr. 55, 247–255.
Oakley, A.J., Lo Bello, M., Nuccetelli, M., Mazzetti, A.P., Parker, M.W., 1999. The ligandin (non-substrate) binding site of human Pi class glutathione transferase is located in the electrophile binding site (H-site). J. Mol. Biol. 291, 913–926.
Olliaro, P., 2001. Mode of action and mechanisms of resistance for antimalarial drugs. Pharmacol. Ther. 89, 207–219.
Otwinowski, Z., Minor, W., 1997. Processing of X-ray diffraction data collected in oscillation mode. Methods Enymol. 276, 307–326.
Perbandt, M., Burmeister, C., Walter, R.D., Betzel, C., Liebau, E., 2004. Native and inhibited structure of a Mu class-related glutathione S-transferase from *Plasmodium falciparum*. J. Biol. Chem. 279, 1336–1342.
Perez, B.C., Teixeira, C., Albuquerque, I.S., Gut, J., Rosenthal, P.J., Gomes, J.R., Prudencio, M., Gomes, P., 2012. N-cinnamoylated chloroquine analogues as dual-stage antimalarial leads. J. Med. Chem.
Perrakis, A., Morris, R., Lamzin, V.S., 1999. Automated protein model building combined with iterative structure refinement. Nat. Struct. Biol. 6, 458–463.
Prade, L., Huber, R., Manoharan, T.H., Fahl, W.E., Reuter, W., 1997. Structures of class pi glutathione S-transferase from human placenta in complex with substrate, transition-state analogue and inhibitor. Structure 5, 1287–1295.

Preu, P., Braun, M., 2014. German SIMBOX on Chinese mission Shenzhou-8: Europe's first bilateral cooperation utilizing China's Shenzhou programme. Acta Astronaut. 94, 584–591.

Quesada-Soriano, I., Baron, C., Tellez-Sanz, R., Garcia-Maroto, F., Garcia-Fuentes, L., 2014. Asn112 in Plasmodium falciparum glutathione S-transferase is essential for induced reversible tetramerization by phosphate or pyrophosphate. Biochim. Biophys. Acta.

Raghunathan, S., Chandross, R.J., Kretsinger, R.H., Allison, T.J., Penington, C.J., Rule, G.S., 1994. Crystal structure of human class mu glutathione transferase GSTM2-2. Effects of lattice packing on conformational heterogeneity. J. Mol. Biol. 238, 815–832.

Reinemer, P., Prade, L., Hof, P., Neuefeind, T., Huber, R., Zettl, R., Palme, K., Schell, J., Koelln, I., Bartunik, H.D., Bieseler, B., 1996. Three-dimensional structure of glutathione S-transferase from *Arabidopsis thaliana* at 2.2 A resolution: structural characterization of herbicide-conjugating plant glutathione S-transferases and a novel active site architecture. J. Mol. Biol. 255, 289–309.

Sinning, I., Kleywegt, G.J., Cowan, S.W., Reinemer, P., Dirr, H.W., Huber, R., Gilliland, G.L., Armstrong, R.N., Ji, X., Board, P.G., et al., 1993. Structure determination and refinement of human alpha class glutathione transferase A1-1, and a comparison with the Mu and Pi class enzymes. J. Mol. Biol. 232, 192–212.

Tripathi, T., Rahlfs, S., Becker, K., Bhakuni, V., 2007. Glutathione mediated regulation of oligomeric structure and functional activity of *Plasmodium falciparum* glutathione S-transferase. BMC Struct. Biol. 7, 67.

Wallace, A.C., Laskowski, R.A., Thornton, J.M., 1995. LIGPLOT: a program to generate schematic diagrams of protein-ligand interactions. Protein Eng. 8, 127–134.

WHO. 2010. World Malaria Report. www.who.int.